Applied Surface Science 610 (2023) 155393

Contents lists available at ScienceDirect

Applied Surface Science

journal homepage: www.elsevier.com/locate/apsusc

Full Length Article

Optimization of multilayer graphene-based gas sensors by ultraviolet photoactivation

Álvaro Peña [a,*], Daniel Matatagui [a,b,e], Filiberto Ricciardella [c], Leandro Sacco [c], Sten Vollebregt [c], Daniel Otero [a], Jesús López-Sánchez [d], Pilar Marín [a,b], Mari Carmen Horrillo [e]

[a] Instituto de Magnetismo Aplicado, UCM-ADIF, 28230 Las Rozas, Spain
[b] Departamento de Física de Materiales, Universidad Complutense de Madrid (UCM), 28040 Madrid, Spain
[c] Department of Microelectronics, Delft University of Technology, Feldmannweg 17, 2628 CT Delft, the Netherlands
[d] Department of Electroceramics, Instituto de Cerámica y Vidrio (ICV), CSIC, 28049 Madrid, Spain
[e] SENSAVAN, Instituto de Tecnologías Físicas y de la Información (ITEFI), CSIC, 28006 Madrid, Spain

ARTICLE INFO

Keywords:
Graphene gas sensors
Ultraviolet
Nitrogen dioxide
Limit of detection
Ammonia
Carbon monoxide

ABSTRACT

Nitrogen dioxide (NO_2) is a potential hazard to human health at low concentrations, below one part per million (ppm). NO_2 can be monitored using gas sensors based on multi-layered graphene operating at ambient temperature. However, reliable detection of concentrations on the order of parts per million and lower is hindered by partial recovery and lack of reproducibility of the sensors after exposure. We show how to overcome these longstanding problems using ultraviolet (UV) light. When exposed to NO_2, the sensor response is enhanced by 290 % – 550 % under a 275 nm wavelength light emitting diode irradiation. Furthermore, the sensor's initial state is completely restored after exposure to the target gas. UV irradiation at 68 W/m2 reduces the NO_2 detection limit to 30 parts per billion (ppb) at room temperature. We investigated sensor performance optimization for UV irradiation with different power densities and target gases, such as carbon oxide and ammonia. Improved sensitivity, recovery, and reproducibility of UV-assisted graphene-based gas sensors make them suitable for widespread environmental applications.

1. Introduction

The hazard to human health of air pollutants derived from human activity has been acknowledged as a problem to be assessed [1]. Among these pollutants, it has been demonstrated that NO_2 presence in the ppb and ppm range causes and exacerbates respiratory complications [2].

Latza et al. found moderate evidence that exposures of 0.1 ppm for 24 h or exposures to an annual mean of 0.026 ppm were related to adverse health effects, including increased hospital admissions and mortality, being children, adolescents, elderly, and asthmatics susceptible population of these effects [3]. A similar annual mean exposure limit (0.021 ppm) was indicated by the World Health Organization [4]. More recently, the National Institute for Occupational Safety and Health (USA) has established a recommended limit of 1 ppm for exposures up to 10 h [5]. In contrast, the American Conference of Governmental Industrial Hygienists recommended limit is 0.2 ppm for exposures up to 8 h [6]. To put these numbers into context, the maximum hourly concentrations measured in urban areas in the UK or the USA are around 0.4–0.5 ppm [7], whereas the median lethal concentration (LC50) for one hour has been estimated at 174 ppm[8]. Although several discrepancies are found throughout the literature regarding the exact value of the exposure limits, monitoring systems capable of warning us against the sub-ppm presence of NO_2 and other pollutants through highly sensitive sensors are an obvious necessity.

Chemiresistive sensors have been widely used to detect NO_2 and other air pollutants. These devices are based on an active material with electrical properties that can experience changes as a reaction to variations in the chemical characteristics of the surrounding environment [9]. Typically, metal oxides have been used as the sensing material. However, metal oxide-based devices require high temperatures for an optimum operation which in turn have high power consumption (tens to hundreds of mW) or complex technological processes for microheater implementation and harm the lifetime of nanostructured materials [10–14].

Graphene is a recent alternative among the different active materials for chemiresistive gas sensors. Since graphene consists of an atom-thick

* Corresponding author.
E-mail address: alvapena@ucm.es (Á. Peña).

https://doi.org/10.1016/j.apsusc.2022.155393
Received 11 August 2022; Received in revised form 6 October 2022; Accepted 18 October 2022
Available online 28 October 2022

layer, every carbon atom is a surface atom. In addition, its large specific surface (2630 m^2/g), high conductivity, and low noise-to-signal ratio make graphene and graphene-based materials ideal candidates for gas sensing applications [15–17].

The first graphene-based gas sensor was reported in just over a decade, with sensitivity down to a single molecule under highly controlled conditions [18]. During the following years, the number of similar devices reported for detecting different gaseous molecular species under conditions closer to real-life applications has increased dramatically [19–22]. These graphene-based devices have demonstrated their potential for sensing NO_2, carbon monoxide (CO), sulfur dioxide (SO_2) or ammonia (NH_3), among other analytes, and significantly, the research interest in the material has increased [8,23–25].

However, a common disadvantage of graphene-based gas sensors is their partial recovery. Briefly, physically adsorbed molecules tend to stick to the surface of the material, occupying adsorption sites that cannot be used to detect incoming molecules. The inability for full recovery reduces the device's sensitivity after each exposition to the analyte [26]. Different forced-desorption methods have been proposed to address the problem, such as thermal annealing [20,27–29] or ultraviolet (UV) irradiation [18,30–32].

Few researchers have tested graphene-based sensors under continuous UV irradiation and reported that along with promoting desorption, UV irradiation also improves the overall sensing performance in terms of faster and larger response [33,34]. However, the mechanisms behind this improvement and the optimal combination between the material's structure and composition, wavelength and intensity of UV, and analytes are not fully understood yet [35].

A recent publication reported improvement in the maximum response of a graphene-based sensor toward water vapors (~420 %), ethanol (~5400 %, from practically zero response) and dimethyl methylphosphonate (~50 %) under continuous UV irradiation [34]. In that paper, three different wavelengths above 365 nm were used, where the material featured a flat optical absorption.

In a previous article [33], we tested a mesoporous graphene-based chemiresistive sensor under continuous UV irradiation using 275 nm wavelength, which is related to electronic transitions in graphene [36,37]. The influence of UV irradiation had a positive effect on the NO_2 sensing performance, resulting in a response to NO_2 increase of 3 %. However, we believe that, due to the agglomerated structure of the material, a sensible amount of the material's active surface was not irradiated, thus showing only a slight enhancement. Henceforth, to acquire a deeper understanding of the UV effect, in this work, we have used a bidimensional graphene-based material, later reported as multilayer graphene (MLG).

We have studied the sensing capabilities of two different MLG-based sensors under 275 nm UV irradiation towards oxidizing and reducing gases. Through the investigation of the right conditions of UV irradiation, we aim at optimizing the sensing performance of MLG-based sensors toward sub-ppm NO2 detection to further pave the way for applying the gas sensors based on two-dimensional materials in the real environment.

2. Materials and methods.

2.1. Material synthesis and characterization

MLG has been synthesized by chemical vapour deposition (CVD) on a pre-patterned Mo catalyst in an AIXTRON BlackMagic Pro reactor [38]. 20 sccm of methane (CH_4) was used as a carbon feedstock for 20 min in Ar/H_2 atmosphere at 25 mbar, and two different values of growth temperature, i.e., 890 °C or 935 °C [38–41].

The grown material was investigated by Raman spectroscopy using a Witec ALPHA model 300RA (Oxford Instruments) with a Nd:YAG green laser source of 532 nm in p-polarization. The optical resolution is ~ 200 nm in lateral and ~ 500 nm in vertical dimensions. Intensity Raman mappings of representative regions were carried out for selected samples with a 100x objective lens (numerical aperture of 0.95). Raman spectra were acquired every 500 nm with an integration time of 1.5 s, using a 600 gr/mm grating with a spectral resolution of ~ 0.02 cm^{-1}. The output laser power employed was 0.2 mW to avoid sample damage or overheating effects [42], previously calibrated with a Thorlabs potentiostat. Raman data were examined and analyzed by the Witec Plus Software (version 2.08).

The surface morphology of the samples after growth was measured by atomic force microscopy (AFM) employing an ND-MDT AURA setup, operating in semi-contact mode with a poly-Si HA-NC cantilever having a radius < 10 nm, at a rate of 0.60 Hz and acquiring 256 lines on scanned areas of 25 μm^2.

2.2. Sensing device preparation

The sensing devices were fabricated by adopting the transfer-free process, further detailed elsewhere [38]. Through a few lithographic steps, a sputtered and patterned Mo layer (50 nm) was wet-etched after the growth of MLG. That way, MLG dropped on the SiO2/Si substrate at the pre-defined positions. The devices are named MLG890 and MLG935 according to the temperature at which the material was grown. Next, the graphene was contacted using 10/100 nm Cr/Au deposited using e-beam evaporation and patterned using a lift-off process.

The current–voltage (I–V) characteristic of the MLG-based resistors has been obtained using a semi-automatic probe station equipped with an Agilent 4156C semiconductor parameter analyzer.

To verify the quality of the deposited materials and the connection to the electrodes, scanning electron microscopy (SEM, Hitachi SU-8230).

2.3. Gas setup

Multilayer graphene-based devices were placed in a 3D-printed PLA airtight cell (with a volume of 14.68 mL) connected to an automated gas generator. The airflow inside the cell was set to 100 $mL \bullet min^{-1}$, and the measurements were performed by exposing the sensor to a mixture of the target gas NO_2, CO, and NH_3 (from 1 ppm, 10 ppm, and 50 ppm balance air cylinders, respectively) and synthetic dry air as a carrier, which was also used for purging. All gases were provided by Nippon Gases (Madrid, Spain). Mass flow controllers adjusted the concentration of each gas sample through custom-made LabView software that simultaneously monitors the device's resistance using a digital multimeter (Keithley 2001). A schematic representation is provided in Fig. 1.

2.4. Methodology

The responsiveness (R%) of the devices was reported as a relative percentage and described as the change of resistance (R) normalized to base resistance (R_0) in absolute value:

$$Responsiveness(\%) = |\Delta R/R_0 * 100| \quad (1)$$

The response was defined as the maximum change in the responsiveness value achieved during the exposure phase. Although this term is often used only when the device's resistance has achieved a steady state, i. e., saturation, it is here used under the previous definition to provide a quantitative parameter to compare the sensor's performance.

Before every test, the devices were stabilized with running air until no significant variations of their resistance were appreciable, i.e., when the device had reached an equilibrium with the carrier gas. These conditions are regarded as initial conditions. R_0 is thus defined as the resistance measured immediately before the first analyte exposure.

It should be noted that the first cycle of each sequence may have some artefacts coming mainly from the gas filling the setup gas lines. The first cycle has not been removed in the results presented in this work, but it was disregarded for the mean value calculations.

A UV light-emitting diode (LED, 275 nm, SeoulViosys CA3535 -

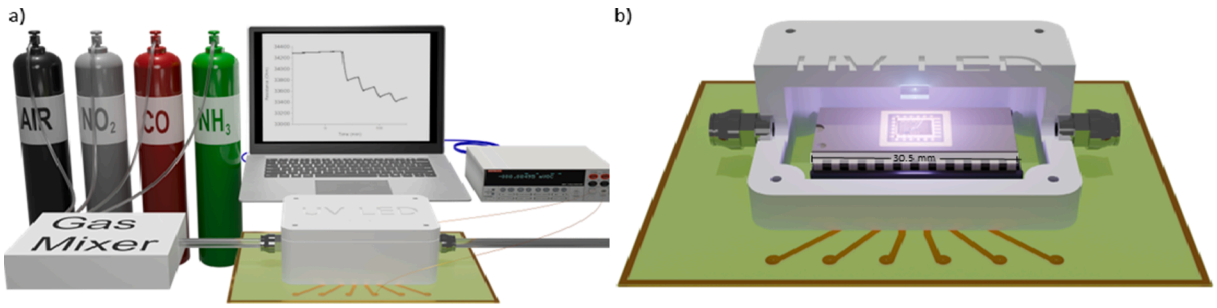

Fig. 1. a) Schematic representation of the experimental setup comprising the cylinders for the gas carrier and analytes, the gas mixer, the data acquisition system, and the sensor's cell; b) detail of the cell with the device and the light emitting diode.

CUD7GF1B) was used to irradiate the sensors during the gas sensing testing. The diode was set at three different operation modes, i.e., 0 % (no irradiation), 50 % and 100 % of its maximum power density (68 W/m^2). These three modes were named UV@OFF, UV@50, and UV@100, respectively. Given that the active layer surface of the devices was 1030 μm^2, the power irradiated into it was 70 nW for UV@100 and 35 nW for UV@50. In addition, a fourth mode, UV@DES, was configured using UV irradiation, at 100 % of the LED power, during the purge phase only.

2.5. Description of the tests

Five sequences (Test1-Test5) were designed to study the sensing behaviour of the devices. Each sequence consists of a baseline step, where only carrier gas is flushed for 60 min (not fully shown in this work); and cycles with a 10-minute exposure phase, when the analyte gas is injected into the sensing chamber and a 20-minute purge phase, exposing the device to the carrier gas only. All tests were performed under standard ambient temperature and pressure conditions. Each test specification is described as follows:

Test1: Four consecutive cycles of 1 ppm of NO_2 under UV@OFF.
Test2: Four consecutive cycles of 1 ppm of NO_2 under UV@100.
Test3: Consecutive cycles with increasing NO_2 concentrations, from 0.2 to 1 ppm in 0.1 ppm steps, under UV@OFF and UV@100.
Test4: Four consecutive cycles with 1 ppm of NO_2, analogously to Test2, with the difference that four different UV configurations have been used, i.e., UV@OFF, UV@50, UV@100, and UV@DES.
Test5: Consecutive cycles with 1 ppm of CO and 10 ppm of NH_3 under UV@OFF, UV@50.

Test1, Test2 and Test3 were performed on devices named MLG890 and MLG935, while Test4 and Test5 were done only on MLG935.

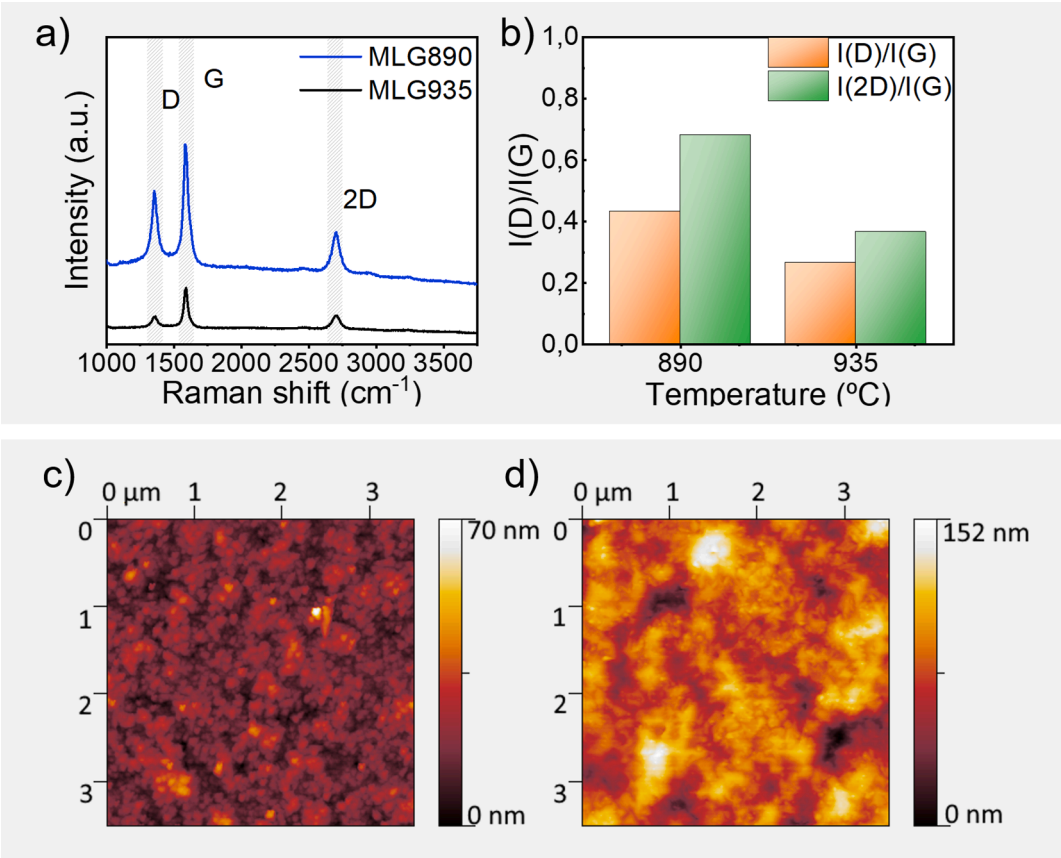

Fig. 2. a) Raman spectra for MLG890 and MLG935, b) I(D)/I(G) and I(2D)/I(G) ratios; AFM images (3.5 µm × 3.5 µm) for c) MLG890 and d) MLG935.

3. Results.

3.1. Material characterization

Fig. 2a shows the average Raman spectra for MLG890 (blue line) and MLG935 (grey line). These spectra were obtained from calculated in-plane Raman intensity images of representative areas (Figure S1). Importantly, D, G, and 2D Raman bands are indicated, in which Lorentzian fits are performed to reveal their I(D)/I(G) and I(2D)/I(G) ratios. The G-band, located around 1580 cm^{-1}, is related to in-plane vibrations of the sp^2 hybridized carbon atoms. The D band, located around 1350 cm^{-1}, comes from vibration near defects or graphene edges. Finally, the 2D band (often referred to as G'), located around 2700 cm^{-1}, is a second-order band related to layer stacking [43,44]. The ratio between the intensities from bands D and G (I(D)/I(G)) decreased from 0.8 to 0.5 for MLG890 and MLG935, respectively, indicating a lower defect density for the latter (Fig. 2b red line). Whereas I(2D)/I(G) remained practically constant with the growing temperature from 0.68 and 0.71 (Fig. 2b red line).

Fig. 2b shows the I(D)/I(G) and I(2D)/I(G) ratios. I(D)/I(G) ratio decreases from 0.433 to 0.266 for growing temperatures of 890 and 935 °C, respectively, indicating a lower defect contribution for the latter [33]. Similarly, I(2D)/I(G) ratio decreases from 0.682 to 0.366. This effect could be related to aggregation effects from the increasing temperature, as shown in Fig. S1.

Fig. 2c and 2d show the AFM 3.5 μm × 3.5 μm images for MLG grown at 890 °C and 935 °C, respectively. The average roughness (R_a) was calculated in three different zones of the deposited MLG. For MLG890, R_a was 5.35 ± 0.05 nm, whereas, for MLG935, R_a was 17.4 ± 0.6 nm.

The resistive character of the devices was confirmed by the lineal I-V behaviour (Fig. S2). In addition, the quality of the contacts between the MLG and the gold electrodes for both devices was verified with SEM (Fig. S3).

3.2. Gas sensing.

Test1 was designed to evaluate the sensing capability of the MLG-based devices toward NO_2 (Fig. 3a and b).

Under exposure to NO_2, devices displayed a decrease in resistance, indicating a p-type behaviour of the MLG, as also observed elsewhere [20,22,41,45,46]. Essentially, when the material is exposed to an oxidizing or electron acceptor molecule, such as NO_2, electronic transfer increases the number of positive charge carriers, i.e., holes, leading to a decrease in the material resistance.

MLG890 exhibited low response (<0.1 %), and changes after each cycle were not distinguishable. However, for MLG935, the response systematically decreased after each cycle. It was also noticed that, during the purge phase, the device did not recover its initial conditions.

To study the effect of UV irradiation on the device's operation, Test2 repeated the conditions of Test1 under UV@100. Results are presented in Fig. 3c and d. It was observed that, under UV irradiation, the responsiveness of both devices remarkably tended to a steady state during the exposure phase differently from Test1. More importantly, both devices showed a larger response than during Test1. For MLG890, the mean response during the exposures drastically increased from 0.07 ± 0.02 % (UV@OFF) to 0.24 ± 0.02 % (UV@100), corresponding to a 340 % increase. For MLG935, a 290 % increase in the mean response was observed, from 0.58 ± 0.15 % to 1.70 ± 0.05 % under UV irradiation. No significant decrease in the response was observed after each cycle.

The most relevant effect of UV irradiation was the full recovery during the purge phase. Under UV@100, both devices could recover to their initial conditions approximately during the first 10 min of the purge phase. Furthermore, no hysteresis is observed after each cycle of exposure at 1 ppm of NO_2, indicating that UV irradiation drastically improves the reproducibility of each exposure step and the reliability of both devices. The effects of the UV irradiation in terms of responsiveness and reproducibility are visible in Fig. 3e and 3f, where the responses of the tested devices after each cycle with (violet dots) and without (black dots) UV irradiation are reported.

The responsiveness time can be evaluated using the τ_{90} parameter, defined as the time required to achieve the 90 % of the response (Fig. S4) [33,47].

Table 1 shows the mean values of τ_{90} as determined from Test1 and Test2. For UV@100, both devices exhibit τ_{90} values approximately 70 %

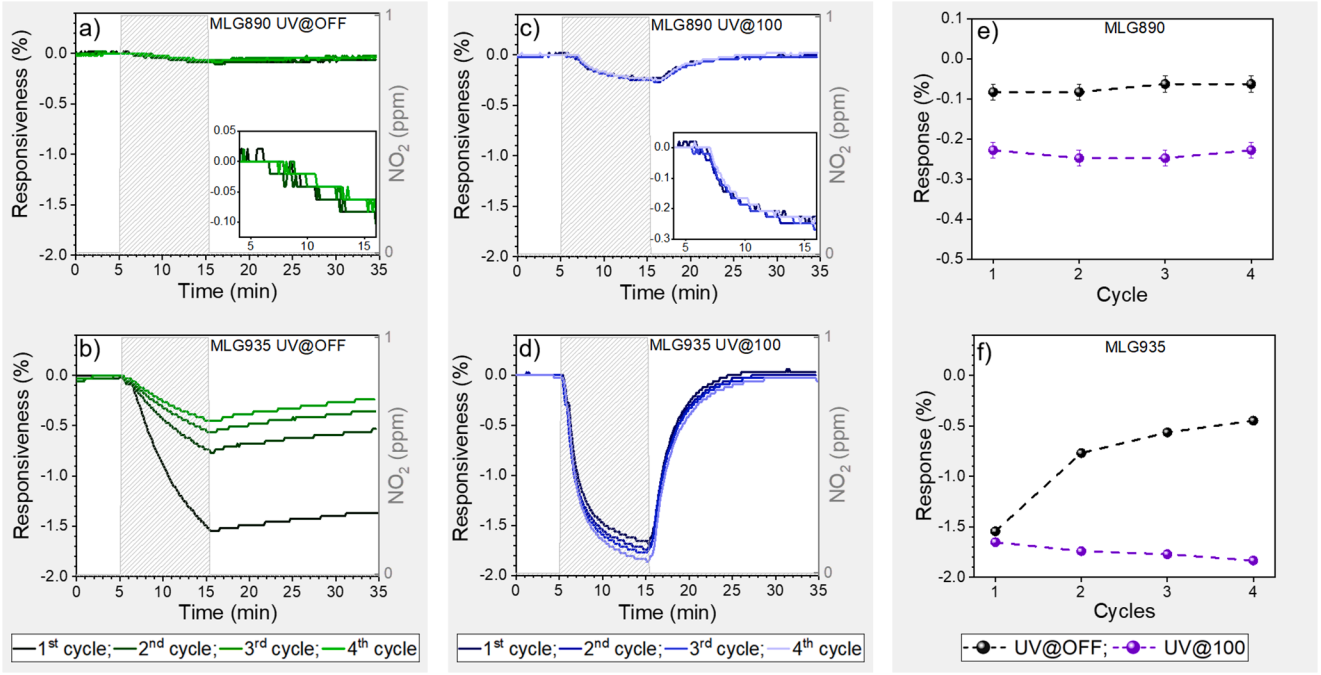

Fig. 3. Real-time responsiveness towards 1 ppm of NO_2 of (a) MLG890 and (b) MLG935 under UV@OFF, and (c) MLG890 and (d) MLG935 under UV@100. The insets of panels a) and c) have the same units of the main graphs the axis magnitudes and represent the zoom of the exposure windows of the main panels. A comparison of the effect of UV irradiation in the response after each cycle is provided in e) and f).

Table 1
τ_{90} parameter extracted from Test1 and Test2.

τ_{90} (minutes)		
UV setting	MLG890	MLG935
UV@OFF	8.4 ± 1.6	8.2 ± 1.0
UV@100	6.4 ± 1.0	5.6 ± 0.3

Table 2
LoD (NO_2) for the devices under UV@100.

Calculations from Test3		
Parameter	MLG890	MLG935
Sensitivity (%/ppm)	0.33 ± 0.03	1.91 ± 0.17
LoD (ppb)	86 ± 3	31 ± 1

lower than those under UV@OFF. The results therefore remarkably show that the sensors achieve the response at a faster rate when exposed to UV irradiation. In the case of UV@OFF, 90 % of the response value is achieved roughly after 8 min, indicating a near-to-linear response under the experiment's conditions. For UV@100, instead, during the first minutes of exposure, the response varies with a steeper slope followed by a more gradual slope, typically related to the saturation process where the device's responsiveness will no longer vary significantly. The 90 % of the response is then reached after about 6 min.

The effect of UV irradiation previously observed was confirmed in Test3 (Fig. 4). Under dark conditions, i.e. UV@OFF, a downward drift with a systematic decrease of the responsiveness displayed that MLG890 and MLG935 suffered partial recovery, starting from the first exposure at 200 ppb. Under UV irradiation, no drift was observed, and the devices started each subsequent exposure phase from the initial conditions, meaning that no hysteresis was observed from two subsequent cycles.

To calibrate the devices and calculate the limit of detection (LoD), the response toward each concentration was extracted from Test3. A linear fit of these values provided the sensitivity (Table 2), i.e., the response to a certain concentration of NO_2 (%/ppm). The LoD was then calculated using the following equation.

$$LoD_{(RMSnoise,\ \mathrm{Sensitivity})} = \frac{3 * RMSnoise}{Sensitivity} \tag{2}$$

RMS noise is the root mean squared noise of a 30 min baseline, i.e., under the continuous flush of the carrier gas in the chamber with no analyte present. The LoD error (ΔLoD) was calculated from equation (2) using uncertainty propagation.

The data for LoD calculation is presented in Fig. 5. For UV@OFF, due to the partial recovery, the response did not increase with the concentration, and the linear fit does not converge to a coherent sensitivity so that the LoD can be calculated (see Fig. S5). Thus, LoD can be calculated only under UV@100 conditions.

For UV@100, the slope gave a sensitivity of 0.3 and 1.9 %/ppm (absolute value) for devices MLG890 and MLG935, respectively. The extrapolated LoD is reported in Table 2. For UV@100, both devices were able to detect sub-ppm of NO_2. Remarkably, the LoD sits in the tens of parts per billion (ppb) range with extremely low error, i.e., below 3 % relative error in both cases.

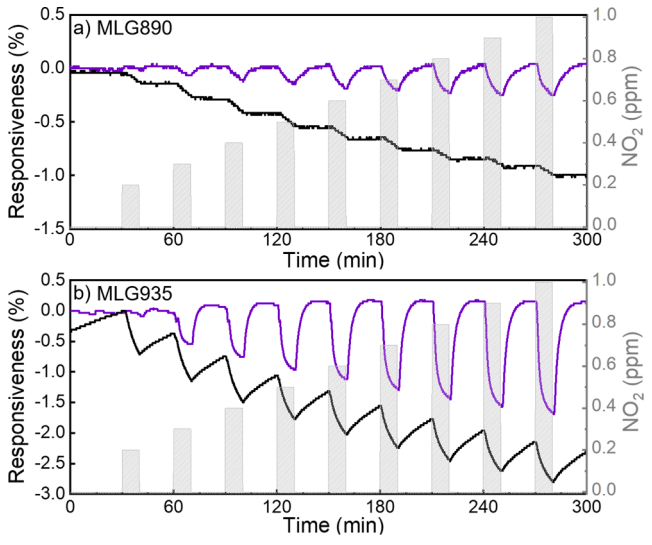

Fig. 4. Real time responsiveness of a) MLG890 and b) MLG935 towards different concentrations of NO_2 under UV@OFF (black line) and UV@100 (purple line).

Test4 was designed to verify the effect of UV irradiation when halving the power density (UV@50) or when irradiating the device during the desorption phase only (UV@DES). This test was carried out on MLG935 as this sensor gave the best results in terms of LoD and sensitivities. Fig. 6a shows the results of the sensor's behaviour under the different UV configurations. Fig. 6b reports the normalized responsiveness for the second cycle of each configuration. The response values measured for Test4 are presented in Table 3, the mean value is also presented in Fig. 6c.

For UV@OFF, MLG935 exhibited the lowest response, 0.73 %. In addition, the device exhibited poor recovery and suffered a downward drift with a decrease in its sensing performance.

For UV@50, MLG935 exhibited extraordinary responsiveness. For all the cycles, the response remains above 3 %, which remarkably results in the highest response observed in this work. During the purge phase, the sensor fully recovered its initial conditions.

For UV@100, MLG935 exhibited a response of around 1.70 % for all cycles. Unlike under other UV conditions, for UV@100 the responsiveness decreased rapidly after the first few minutes of exposure, approaching a plateau around the maximum value. The sensor fully recovered its initial conditions and excellent reproducibility was observed across the different cycles.

Finally, For UV@DES, MLG935 exhibited a large response, around 2.5 %. The responsiveness is more pronounced than under UV@OFF, achieving a behavior between UV@100 and UV@50, despite being irradiated only during the exposure phase. During the purge phase, the recovery reached ~ 90 % of the initial conditions.

Regarding the responsiveness time, UV@OFF and UV@DES exhibited a similar τ_{90}, around 8 min. The fastest time was achieved for UV@100, at around 5.5 min, followed by UV@50, at around 6 min (see Fig. 6d).

Results from Test4 revealed that under UV irradiation, regardless of the specific configuration, MLG935's sensing performance was enhanced regarding its responsiveness to NO_2 and the recovery of the initial conditions during the purge phase. Since the different UV irradiation conditions led to different results, Test4 showed that determining the UV irradiation required to achieve the best sensing performance for the sensor is not trivial. Establishing the optimal UV configuration might lead to a significant breakthrough in the scenario of the gas sensors working in environmental conditions.

Test5 was designed to verify the effect of UV irradiation on gaseous species of different chemical nature, i.e., reducing gases, such as CO and NH_3 (Fig. 7). The UV irradiation was set at UV@50 configuration due to the promising results of Test4.

MLG935 showed increased resistance when exposed to the reducing gases, further confirming the p-type behaviour, along with previous results towards NO_2. Essentially, when exposed to a reducing or electron donor molecule, such as CO or NH_3, electronic transfer decreases the number of holes, increasing the material's resistance [22,33,39,48,49].

For both gases, UV irradiation at UV@50 led to a threefold response enhancement (Table S1). For the second and subsequent cycles, MLG935 exhibited slight variation in the response and fully recovered the initial

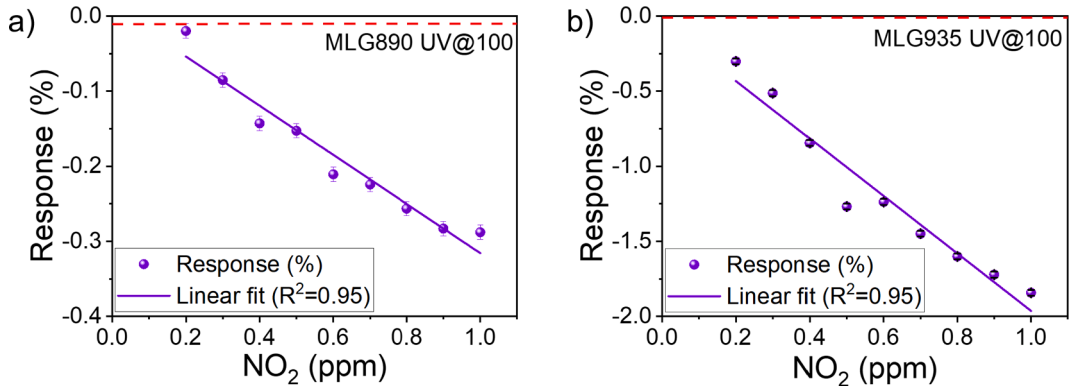

Fig. 5. Calibration curve for a) MLG890 and b) MLG935, towards different concentrations of NO_2 under UV@100. The dotted red line represents the RMSnoise value used in Eq. (2).

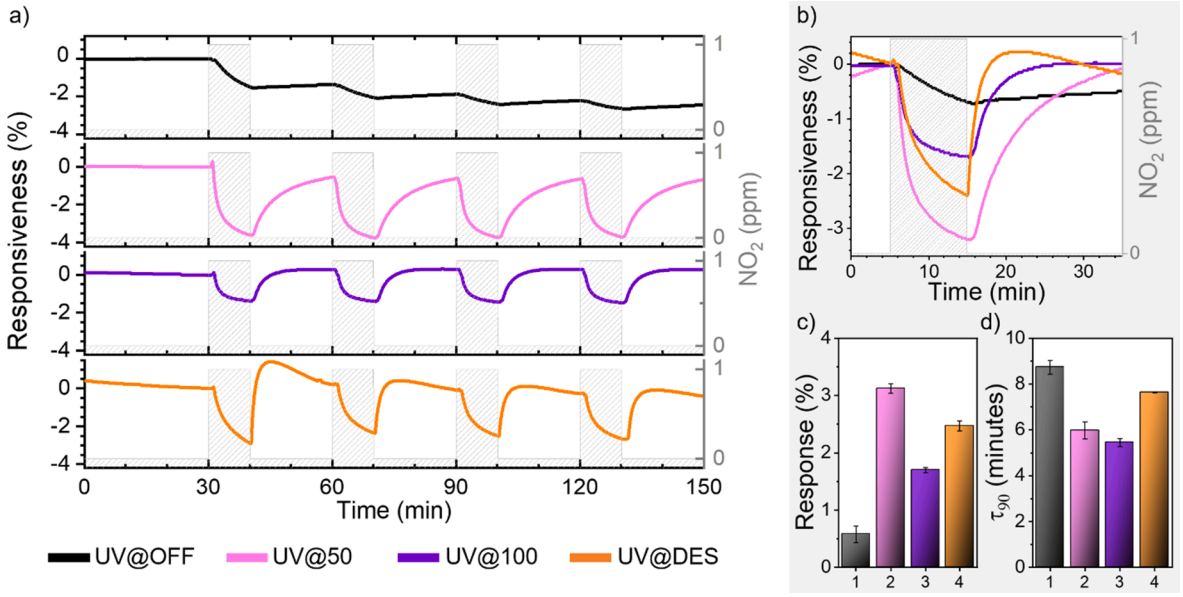

Fig. 6. a) Real time responsiveness of MLG935 towards 1 ppm of NO_2 under different UV irradiation settings and b) the second cycle extracted and normalized. c) Mean values of the response and d) mean values of τ_{90} obtained from Test4.

Table 3
Response and τ_{90} of MLG935 towards 1 ppm of NO_2 under different UV irradiation configurations.

NO_2	UV setting	2nd cycle	3rd cycle	4th cycle	Mean ± SD
Response (%)	UV@OFF	0.73	0.56	0.44	0.58 ± 0.15
	UV@50	3.21	3.12	3.04	3.12 ± 0.08
	UV@100	1.69	1.66	1.75	1.70 ± 0.05
	UV@DES	2.57	2.43	2.41	2.47 ± 0.09
τ_{90} (min)	UV@OFF	8.75	9.03	8.44	8.74 ± 0.30
	UV@50	5.65	5.92	6.38	5.98 ± 0.37
	UV@100	5.62	5.28	5.44	5.45 ± 0.17
	UV@DES	7.63	7.67	7.62	7.64 ± 0.02

conditions during the purge phase, regardless of the UV irradiation, in contrast to the results from Test1 and Test2 for NO_2.

4. Discussion

The results have shown that both MLG-based devices suffered a change in their conductivity under gas exposure, mainly caused by a charge transfer mechanism between the gaseous molecules and the graphene's surface [20,22,41,46]. In particular, the devices exhibited a p-type behaviour, as demonstrated by exposing the devices to an oxidizing analyte (NO_2) and two reducing analytes (CO and NH_3). Briefly, NO_2 acted as an electron acceptor, trapping electrons from the conduction band and decreasing the MLG's resistivity. Conversely, CO and NH_3 acted as electron donors, neutralizing the positive charge carriers and thus increasing the MLG's resistivity. Furthermore, this behaviour was observed in both cases without UV irradiation (Test1 and Test5) and with different UV irradiation configurations (Test2-Test5).

Regarding the NO_2 detection, both devices reacted to the exposure at 1 ppm without UV irradiation (UV@OFF), regardless of their synthesis parameters and structural characteristics. However, both sensors suffered from a partial recovery negatively impacted the reliability of the quantitative measurements of NO_2 (Test1).

However, the difference in their material's structural characteristics could significantly contribute to the interaction with NO_2 and their sensing performances. As observed from the Raman spectra, MLG890 and MLG935 differ in defect density, probably due to the growth conditions [46]. In particular, MLG890, which presents a higher I(D)/I(G) ratio, has a greater defect contribution than MLG935. Noteworthy, in this context, the term defect relates to any disruption of the graphene's lattice, including edges, vacancies, and eventual structural defects.

It is well-known that defects can affect the performance of graphene-

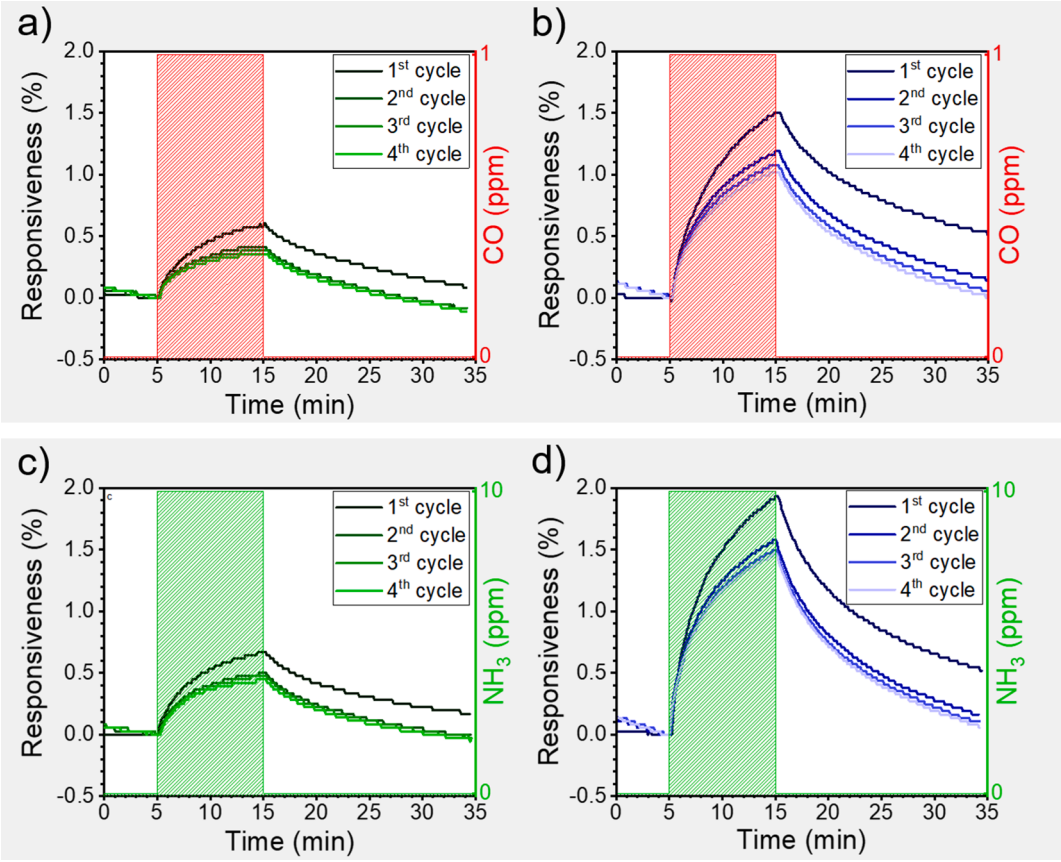

Fig. 7. Real time responsiveness of MLG935 towards 1 ppm of CO performed under a) UV@OFF and b) UV@50, and towards 10 ppm of NH_3 performed under c) UV@OFF and d) UV@50.

based sensors [32,50–53]. On the one hand, it is generally considered that few defects can improve the sensing capabilities of pristine graphene, whereas a large number of defects can significantly damage the lattice and disrupt the sensing performance [54,55]. On the other hand, defects are considered high-energy binding sites to the incoming gaseous molecules compared to the basal plane, affecting adsorption and desorption dynamics. In particular, the presence of defects is related to a slower response and longer recovery times, whereas the response is generally faster for no-defective graphene, namely with lower binding energies [46].

In this work, MLG935 exhibited better responsiveness to NO_2 than MLG890, despite the former being less defective than the latter, in close agreement with a previous report further confirming the hypothesis that defects in graphene play an essential role in the gas sensing application [56]. The exact effects of graphene defects in gas sensing are not yet fully understood, as proved by the examples provided in Table 4 and fall out of the scope of the current work. Nevertheless, our results confirmed that MLG935 was a better candidate to study the effects of UV irradiation.

Under UV irradiation, different gas sensing dynamics were observed. A steeper slope during the first few minutes of exposure was observed for both sensors under UV@100. The responsiveness then approached a steady state with a slower variation. This stabilization of the responsiveness under gas exposure is typically related to a saturation process (Test2). The different slopes and the enabling of a steady state clearly indicated that different adsorption mechanisms took place under UV irradiation [41,57].

This change in the sensing dynamics under UV irradiation had two significant effects that are crucial to the potential application of the devices. Mainly a substantial increase in the responsiveness during the exposure to NO_2 and better recovery of the initial conditions afterwards.

The response of the devices was increased by comparing the mean values for several cycles. For instance, results from Test4 demonstrated an increment of 290 % (UV@100) – 550 % (UV@50) compared to the response toward NO_2 without UV. A similar increase was observed by exposing the sensors to reducing molecules, 270 % and 300 % for CO and NH_3, respectively. Such increases were consistent with the few examples of graphene-based gas sensors operating under continuous UV exposure previously reported (Table 4).

The response enhancement is directly related to the increase in the device's sensitivity and ultimately lowers the LoD. UV irradiation led to a limit of NO_2 as low as 30 ppb for MLG935, enabling to monitor NO_2 below the human toxicity threshold in practical scenarios.

The effect of UV irradiation on the performance of graphene-based gas sensors can be explained through two main mechanisms that occur simultaneously: The photogeneration of electron-hole pairs and the photodesorption of contaminants, often referred to as in-situ cleaning [35,58].

The incident photons create photogenerated electron-hole pairs. For graphene, the photogeneration is caused by absorption in the 275 nm wavelength, related to π-π* electron promotion, according to the following relation [36,37]:

$$h\nu \rightarrow e^{-}_{(h\nu)} + h^{+}_{(h\nu)} \quad (3)$$

The photogenerated charge carriers can then interact with adsorbed molecules, such as water and oxygen species, both electron donors, and cause photodesorption [30,59,60]:

$$h^{+}_{(h\nu)} + O^{-}_{2(ads)} \rightarrow O_{2(gas)} \quad (4)$$

Since the experiments used air as a carrier, the photogenerated electron can promote the additional adsorption of oxygen, leading to highly reactive photoinduced oxygen ions [61]:

Table 4
Collection of previously reported graphene-based gas sensors with different approaches (material, defect engineering and UV irradiation use). Noteworthy for the sake of comparison, the term "graphene" in the table is used in its common acceptation.

Material	Main approach	Analyte	Response	UV impact /Other (if no UV use)	Ref.
Funtionalised rGO	Magnetically aligned; Recovery under UV: 80 mW/cm^2	NO_2/ Air 1 ppm	155 %	Sensor achieved full recovery under UV with neglectable side effects.	[66]
rGO		NO_2/ N_2 5 ppm	13 %		[21]
		NH_3/ N_2 5 ppm	2.5 %		
CNT	Continuous UV: 253.7 nm, 1.7 mW/ cm^2	NO/Air 200 ppm	36 %	5-fold increase but reduced lifetime under UV and material removal.	[67]
Mechanical exfoliation-Graphene	Pristine	NO_2/ N_2 100 ppm	11 %	Sensor achieved full recovery under UV with neglectable side effects.	[55]
	Defective graphene (I (D)/I(G) = 0.24)	NO_2/ N_2 100 ppm	32 %		
	Defective graphene (I (D)/I(G) = 0.59)	NO_2/ N_2 100 ppm	18 %		
Graphite		NO_2/ Air 0.5 ppm	3.32 %		[33]
Ball-milled graphene	Continuous UV: 275 nm	NO_2/ Air 0.5 ppm	14.52 %	Slight improve in response and recovery under UV	
Ball-milled graphene		NO_2/ Air 0.5 ppm	15.97 %		
CVD-graphene		CO/Air 100 ppm	3 %		[22]
		NO_2/ Air 100 ppm	18 %		
CVD-graphene	High temperature operation (150°C)	NH_3/ Air 65 ppm	2.1 %		[48]
CVD-graphene	Heat (200°C) and vacuum to force desorption	NO_2/ Air 10 ppm	15 %		[49]
		NH_3/ Air 10 ppm	17.5 %		
CVD-graphene	Pristine	NO_2/ Air 100 ppm	9.6 %		[52]
	Defective graphene (I (D)/I(G) = 0.04)		15 %		
	Defective graphene (I (D)/I(G) = 0.12)		20 %		
	Defective graphene (I (D)/I(G) = 0.38)		13.3 %		
	Defective graphene (I (D)/I(G) = 1)		7.8 %		
CVD-graphene	Pristine	NO_2/ He 200 ppm	40 %		[51]
		NH_3/ He 200 ppm	3.5 %		
	Defective graphene (I (D)/I(G) = 0.1–1.1)	NO_2/ He 200 ppm	53 %		
		NH_3/ He 200 ppm	25 %		
Commercial graphene substrate	Pristine	NO_2/ Air 5 ppm	9.75 %	Continuous high-temperature operation 150°C was used to improve recovery	[54]
	Defective graphene (I (D)/I(G) = 0.065)	NO_2/ Air 5 ppm	9.1 %		
CVD-graphene	Pristine	NO_2/ Air 100 ppm	20 %		[50]
	Defective graphene (I (D)/I(G) = 0.459)		50 %		
	Defective graphene (I (D)/I(G) = 1.428)		80 %		
CVD-graphene on a flexible substrate	Recovery under UV: 254 nm, 2.5 mW/cm^2	NO_2/ Air 2.5 ppm	65 %	Sensor achieved full recovery under UV with neglectable side effects.	[32]
CVD-graphene	Continuous UV: 370 nm	NH_3/ N_2 0.6 ppm	1.89 %	10-fold increase	[30]
CVD-graphene	Continuous UV: 253.7 nm, 1.7 mW/ cm^2	NO_2/ N_2 0.4 ppb	3.6 %	UV significantly lowered the LoD with neglectable side effects.	[60]
		NH_3/Ar 2 ppb	1.4 %		
CVD-graphene	Continuous UV: 265 nm, 1.68 mW/cm^2	NO_2/ Air 100 ppm	26 %	7-fold increase	[62]
		NH_3/ Air 100 ppm	1.6 %	3-fold increase	
		CO/Air 100 ppm	1.2 %	6-fold increase	
CVD-graphene	Continuous UV: 275 nm, 3.4 mW/cm^2	NO_2/ Air 1 ppm	3.1 %	5-fold increase	This work
	Continuous UV: 275 nm, 6.8 mW/cm^2		1.7 %	3-fold increase	
	Continuous UV: 275 nm, 3.4 mW/cm^2	CO/Air 10 ppm	1.2	3-fold increase	
		NH_3/ Air 10 ppm	1.7	3-fold increase	

$$O_{2(gas)} + e^-_{(hv)} \rightarrow O^-_{2(hv)} \quad (5)$$

These reactive ions can act as binding sites for the analytes with higher affinity to graphene, like NO_2 [62,63]:

$$2NO_{2(gas)} + O^-_{2(hv)} + e^-_{(hv)} \rightarrow 2NO^-_{2(ads)} + O_{2(gas)} \quad (6)$$

Meanwhile, the adsorption mechanisms that operate no irradiation conditions, i.e., the charge transfer from analytes, still occurs under UV irradiation but are further promoted by the excess of charge carriers from the photogeneration process [62,63].

The reversibility of the adsorption mechanisms was observed during the gas sensing tests. UV irradiation significantly promoted the full recovery of the initial conditions for both devices after the exposition to NO_2, improving reproducibility under serial cycles (Test2-Test4). However, for reducing analytes, it was observed that partial recovery was neglectable both with and without UV irradiation (Test5).

Furthermore, no permanent damage from the UV irradiation was observed in the sensors. On the one hand, additional Raman characterization revealed no significant changes in the I(D)/I(G) ratio in a MLG890 sample at before and after UV irradiation conditions (0.433 and 0.432, respectively, see Fig. S1). On the other hand, AFM revealed no significant variation in the roughness of the before and after MLG890 (see Fig. S6). Thus, this confirms that after the photogenerated carriers recombine, the graphene layer returns to its pre-irradiated state with neglectable permanent damages [31–34,55,60,64,65].

Finally, Test4 demonstrated that tuning the power and timing of the UV irradiation configuration is not so trivial, as the best performance in terms of the responsiveness of MLG935 towards NO_2 was obtained for UV@50, followed by UV@DES. Bearing in mind these results, it is very likely that better sensing performance and even lower LoD can be achieved while simultaneously reducing the power requirements. However, the proper mechanisms relating the irradiation intensity with the performance variation are not fully understood yet and will be further investigated.

5. Conclusions

We have presented UV-assisted multilayer graphene-based sensors ultrasensitive to NO_2. The sensors exhibited high sensitivity with limits of detection as low as 30 ppb of NO_2 and full recovery in environmental conditions. Further optimizing the UV configuration, this LoD could be lowered down to ~ 15 ppb.

We proved the effects of UV irradiation toward oxidizing molecules, such as NO_2, and for reducing gases, such as CO and NH_3. We observed a response enhancement of 270 % and 300 % for CO and NH_3, respectively.

This work has also proven that the use of UV irradiation during the sensor's operation is not trivial. Furthermore, it was demonstrated that higher optical output intensity is not directly related to better sensing response, as the response was doubled while halving the UV irradiation. Further studies are required to determine the optimum equilibrium between the UV configuration and the device's performance.

Although the exact mechanisms of how UV irradiation improves the sensing performance is unclear, yet several mechanisms have been proposed. Some of them would promote analyte adsorption, while others would promote desorption. According to our findings, both types of mechanisms may be happening simultaneously, and the equilibrium point between them can be tuned through the UV irradiation configuration to optimize the sensor's operation.

The results hereby presented provide further insights into the underlying mechanisms of UV-assisted sensors.

Funding

Author A. P. received funding from grant PRE2019-0875001234, Ministerio de Ciencia e Innovación (MCI), Spain. D. M. received funding from Comfuturo, Consejo Superior de Investigaciones Científicas, Spain. Authors A. P., D. M., D. O., P. M., and M−C. H. received funding from projects RTI2018-095856-B-C21 and –C22, Ministerio de Ciencia e Innovación, Spain. A. P. and P. M. received funding S2018/NMT-4321, Comunidad de Madrid. J. L.-S. received funding from project PID2020-114192RB-C41, Ministerio de Asuntos Económicos y Transformación Digital (MINECO).

CRediT authorship contribution statement

Álvaro Peña: Conceptualization, Data curation. **Daniel Matatagui:** Conceptualization, Data curation. **Filiberto Ricciardella:** Conceptualization. **Leandro Sacco:** Conceptualization. **Sten Vollebregt:** Conceptualization. **Daniel Otero:** Data curation. **Jesús López-Sánchez:** . **Pilar Marín:** Conceptualization. **M. Carmen Horrillo:** Conceptualization.

Declaration of Competing Interest

The authors declare that they have no known competing financial interests or personal relationships that could have appeared to influence the work reported in this paper.

Data availability

Data will be made available on request.

Acknowledgements

A. P. acknowledges the support of A. Mascaraque, M. A. Barrio, and J. Marqués during the revision process. F.R. acknowledges the Delft University of Technology Else Kooi Lab staff for the processing support. All gas sensing tests were done at SENSAVAN's laboratory. AFM characterization presented in Fig. S6 was done by Jorge Marqués from Instituto de Ciencia de Materiales, Spain. Colour blindness accessibility was considered in the figures. The authors declare no competing financial interest.

Appendix A. Supplementary data

Supplementary data to this article can be found online at https://doi.org/10.1016/j.apsusc.2022.155393.

References

[1] European Commission, Recommendation from the Scientific Committee on Occupational Exposure Limits for Nitrogen Dioxide, 2014.
[2] T.W. Hesterberg, W.B. Bunn, R.O. McClellan, A.K. Hamade, C.M. Long, P. A. Valberg, Critical review of the human data on short-term nitrogen dioxide (NO2) exposures: evidence for NO_2 no-effect levels, Crit. Rev. Toxicol. 39 (2009) 743–781, https://doi.org/10.3109/10408440903294945.
[3] U. Latza, S. Gerdes, X. Baur, Effects of nitrogen dioxide on human health: Systematic review of experimental and epidemiological studies conducted between 2002 and 2006, Int. J. Hyg. Environ. Health 212 (2009) 271–287, https://doi.org/10.1016/j.ijheh.2008.06.003.
[4] World Health Organization (WHO), Nitrogen Oxides (Environmental Health Criteria: 188), 2nd ed., 1997.
[5] The National Institute for Occupational Safety and Health (NIOSH), Centers for Disease Control and Prevention (CDC), NIOSH Pocket guide to chemical hazards, 3rd ed., 2007. http://www.cdc.gov/niosh/npg/npg.html.
[6] American Conference of Governmental Industrial Hygienists (ACGIH), TLVs ® and BEIs ® Based on the Documentation of the ® Defining the Science of Occupational and Environmental Health ® Threshold Limit Values for Chemical Substances and Physical Agents Biological Exposure Indices, Cincinnati, OH, USA, 2019.
[7] World Health Organization (WHO), Air Quality Guidelines for Europe, 2nd ed., WHO regional publications, 2000.
[8] M.d. Khan, M. Rao, Q. Li, Recent advances in electrochemical sensors for detecting toxic gases: NO_2, SO_2 and H_2S, Sensors (Switzerland) 19 (4) (2019) 905, https://doi.org/10.3390/s19040905.
[9] J. Gutiérrez, M.C. Horrillo, Advances in artificial olfaction: Sensors and applications, Talanta 124 (2014) 95–105, https://doi.org/10.1016/j.talanta.2014.02.016.

[10] X. Liu, S. Cheng, H. Liu, S. Hu, D. Zhang, H. Ning, A survey on gas sensing technology, Sensors (Switzerland). 12 (2012) 9635–9665, https://doi.org/10.3390/s120709635.

[11] C. Zhang, A. Boudiba, P. de Marco, R. Snyders, M.G. Olivier, M. Debliquy, Room temperature responses of visible-light illuminated WO3 sensors to NO2 in sub-ppm range, Sens Actuators B Chem. 181 (2013) 395–401, https://doi.org/10.1016/j.snb.2013.01.082.

[12] Q. Li, W. Zeng, Y. Li, Metal oxide gas sensors for detecting NO_2 in industrial exhaust gas: recent developments, Sens Actuators B Chem. 359 (2022) 131579, https://doi.org/10.1016/j.snb.2022.131579.

[13] F. Rasch, V. Postica, F. Schütt, Y.K. Mishra, A.S. Nia, M.R. Lohe, X. Feng, R. Adelung, O. Lupan, Highly selective and ultra-low power consumption metal oxide based hydrogen gas sensor employing graphene oxide as molecular sieve, Sens Actuators B Chem. 320 (2020) 128363, https://doi.org/10.1016/j.snb.2020.128363.

[14] J. Burgués, S. Marco, Low power operation of temperature-modulated metal oxide semiconductor gas sensors, Sensors (Switzerland). 18 (2) (2018) 339, https://doi.org/10.3390/s18020339.

[15] Y. Zhu, S. Murali, W. Cai, X. Li, J.W. Suk, J.R. Potts, R.S. Ruoff, Graphene and graphene oxide: Synthesis, properties, and applications, Adv. Mater. 22 (2010) 3906–3924, https://doi.org/10.1002/adma.201001068.

[16] F. Yavari, N. Koratkar, Graphene-based chemical sensors, J. Phys. Chem. Lett. 3 (2012) 1746–1753, https://doi.org/10.1021/jz300358t.

[17] S. Basu, P. Bhattacharyya, Recent developments on graphene and graphene oxide based solid state gas sensors, Sens Actuators B Chem. 173 (2012) 1–21, https://doi.org/10.1016/j.snb.2012.07.092.

[18] F. Schedin, A.K. Geim, S.V. Morozov, E.W. Hill, P. Blake, M.I. Katsnelson, K. S. Novoselov, Detection of individual gas molecules adsorbed on graphene, Nat. Mater. 6 (9) (2007) 652–655.

[19] J.T. Robinson, F.K. Perkins, E.S. Snow, Z. Wei, P.E. Sheehan, Reduced graphene oxide molecular sensors, Nano Lett. 8 (2008) 3137–3140, https://doi.org/10.1021/nl8013007.

[20] Y. Dan, Y. Lu, N.J. Kybert, Z. Luo, A.T.C. Johnson, Intrinsic response of graphene vapor sensors, Nano Lett. 9 (2009) 1472–1475, https://doi.org/10.1021/nl8033637.

[21] J.D. Fowler, M.J. Allen, V.C. Tung, Y. Yang, R.B. Kaner, B.H. Weiller, Practical chemical sensors from chemically derived graphene, ACS Nano 3 (2009) 301–306, https://doi.org/10.1021/nn800593m.

[22] R.K. Joshi, H. Gomez, F. Alvi, A. Kumar, Graphene films and ribbons for sensing of O_2, and 100 ppm of CO and NO_2 in practical conditions, J. Phys. Chem. C 114 (2010) 6610–6613, https://doi.org/10.1021/jp100343d.

[23] R. Ghosh, M. Aslam, H. Kalita, Graphene derivatives for chemiresistive gas sensors: a review, Mater. Today Commun. 30 (2022) 103182.

[24] F. Perreault, A. Fonseca De Faria, M. Elimelech, Environmental applications of graphene-based nanomaterials, Chem. Soc. Rev. 44 (2015) 5861–5896, https://doi.org/10.1039/c5cs00021a.

[25] K.R. Ratinac, W. Yang, S.P. Ringer, F. Braet, Toward ubiquitous environmental gas sensors - Capitalizing on the promise of graphene, Environ. Sci. Technol. 44 (2010) 1167–1176, https://doi.org/10.1021/es902659d.

[26] N. Iqbal, A. Afzal, N. Cioffi, L. Sabbatini, L. Torsi, NOx sensing one- and two-dimensional carbon nanostructures and nanohybrids: progress and perspectives, Sens Actuators B Chem. 181 (2013) 9–21, https://doi.org/10.1016/j.snb.2013.01.089.

[27] Y.C. Lin, C.C. Lu, C.H. Yeh, C. Jin, K. Suenaga, P.W. Chiu, Graphene annealing: how clean can it be? Nano Lett. 12 (2012) 414–419, https://doi.org/10.1021/nl203733r.

[28] L. Yu, L. Wang, W. Xu, L. Chen, M. Fu, J. Wu, D. Ye, Adsorption of VOCs on reduced graphene oxide, J. Environ. Sci. (China) 67 (2018) 171–178, https://doi.org/10.1016/j.jes.2017.08.022.

[29] X. Deng, T. Gao, J. Dai, Temperature dependence of adsorption and desorption dynamics of NO_2 molecule on boron-doped graphene, Phys. E Low Dimens. Syst. Nanostruct. 137 (2022) 115083.

[30] C.M. Yang, T.C. Chen, Y.C. Yang, M.C. Hsiao, M. Meyyappan, C.S. Lai, Ultraviolet illumination effect on monolayer graphene-based resistive sensor for acetone detection, Vacuum 140 (2017) 89–95, https://doi.org/10.1016/j.vacuum.2016.08.006.

[31] C.M. Yang, T.C. Chen, Y.C. Yang, M. Meyyappan, Annealing effect on UV-illuminated recovery in gas response of graphene-based NO_2 sensors, RSC Adv. 9 (2019) 23343–23351, https://doi.org/10.1039/c9ra01295h.

[32] S. Kumar, S. Kaushik, R. Pratap, S. Raghavan, Graphene on paper: a simple, low-cost chemical sensing platform, ACS Appl. Mater. Interfaces 7 (2015) 2189–2194, https://doi.org/10.1021/am5084122.

[33] D. Matatagui, J. López-Sánchez, A. Peña, A. Serrano, A. del Campo, O.R. de la Fuente, N. Carmona, E. Navarro, P. Marín, M. del Carmen Horrillo, Ultrasensitive NO_2 gas sensor with insignificant NH_3-interference based on a few-layered mesoporous graphene, Sens Actuators B Chem. 335 (2021) 129657.

[34] J. Park, R. Rautela, N. Alzate-Carvajal, S. Scarfe, L. Scarfe, L. Alarie, A. Luican-Mayer, J.M. Ménard, UV illumination as a method to improve the performance of gas sensors based on graphene field-effect transistors, ACS Sens. 6 (2021) 4417–4424, https://doi.org/10.1021/acssensors.1c01783.

[35] R. Kumar, X. Liu, J. Zhang, M. Kumar, Room-Temperature gas sensors under photoactivation: from metal oxides to 2D materials, Nanomicro Lett. 12 (2020), https://doi.org/10.1007/s40820-020-00503-4.

[36] S. Uran, A. Alhani, C. Silva, Study of ultraviolet-visible light absorbance of exfoliated graphite forms, AIP Adv. 7 (3) (2017) 035323.

[37] F.T. Johra, J.W. Lee, W.G. Jung, Facile and safe graphene preparation on solution based platform, J. Ind. Eng. Chem. 20 (2014) 2883–2887, https://doi.org/10.1016/j.jiec.2013.11.022.

[38] S. Vollebregt, B. Alfano, F. Ricciardella, A.J.M. Giesbers, Y. Grachova, H.W. van Zeijl, T. Polichetti, P.M. Sarro, A transfer-free wafer-scale CVD graphene fabrication process for MEMS/NEMS sensors, in: 2016 IEEE 29th International Conference on Micro Electro Mechanical Systems (MEMS). (2016).

[39] F. Ricciardella, S. Vollebregt, T. Polichetti, B. Alfano, E. Massera, P.M. Sarro, High sensitive gas sensors realized by a transfer-free process of CVD graphene, in: Proceedings of IEEE Sensors, Institute of Electrical and Electronics Engineers Inc., 2017. https://doi.org/10.1109/ICSENS.2016.7808638.

[40] F. Ricciardella, T. Polichetti, S. Vollebregt, B. Alfano, E. Massera, P.M. Sarro, Analysis of a calibration method for non-stationary CVD multi-layered graphene-based gas sensors, Nanotechnology 30 (2019), https://doi.org/10.1088/1361-6528/ab2aac.

[41] F. Ricciardella, S. Vollebregt, T. Polichetti, M. Miscuglio, B. Alfano, M.L. Miglietta, E. Massera, G. di Francia, P.M. Sarro, Effects of graphene defects on gas sensing properties towards NO_2 detection, Nanoscale 9 (2017) 6085–6093, https://doi.org/10.1039/c7nr01120b.

[42] J. López-Sánchez, A. Serrano, A. del Campo, Á. Muñoz-Noval, E. Salas-Colera, M. Cabero, M. Varela, M. Abuín, G.R. Castro, J. Rubio-Zuazo, Ó. Rodríguez de la Fuente, N. Carmona, A combined micro-Raman, X-ray absorption and magnetic study to follow the glycerol-assisted growth of epsilon-iron oxide sol-gel coatings, J. Alloy. Compd. 892 (2022) 162061, https://doi.org/10.1016/j.jallcom.2021.162061.

[43] L.M. Malard, M.A. Pimenta, G. Dresselhaus, M.S. Dresselhaus, Raman spectroscopy in graphene, Phys. Rep. 473 (2009) 51–87, https://doi.org/10.1016/j.physrep.2009.02.003.

[44] R. Muzyka, S. Drewniak, T. Pustelny, M. Chrubasik, G. Gryglewicz, Characterization of graphite oxide and reduced graphene oxide obtained from different graphite precursors and oxidized by different methods using Raman spectroscopy, Materials 11 (2018) 15–17, https://doi.org/10.3390/ma11071050.

[45] F. Ricciardella, K. Lee, T. Stelz, O. Hartwig, M. Prechtl, M. McCrystall, N. McEvoy, G.S. Duesberg, Calibration of nonstationary gas sensors based on two-dimensional materials, ACS Omega 5 (2020) 5959–5963, https://doi.org/10.1021/acsomega.9b04325.

[46] F. Ricciardella, S. Vollebregt, R. Tilmann, O. Hartwig, C. Bartlam, P.M. Sarro, H. Sachdev, G.S. Duesberg, Influence of defect density on the gas sensing properties of multi-layered graphene grown by chemical vapor deposition, Carbon Trends. 3 (2021), 100024, https://doi.org/10.1016/j.cartre.2021.100024.

[47] D. Matatagui, C. Cruz, F. Carrascoso, A.M. Al-Enizi, A. Nafady, A. Castellanos-Gomez, M.D.C. Horrillo, Eco-Friendly disposable WS2 paper sensor for Sub-ppm NO_2 detection at room temperature, Nanomaterials 12 (7) (2022) 1213.

[48] M. Gautam, A.H. Jayatissa, Gas sensing properties of graphene synthesized by chemical vapor deposition, Mater. Sci. Eng., C 31 (2011) 1405–1411, https://doi.org/10.1016/j.msec.2011.05.008.

[49] F. Yavari, E. Castillo, H. Gullapalli, P.M. Ajayan, N. Koratkar, High sensitivity detection of NO_2 and NH_3 in air using chemical vapor deposition grown graphene, Appl. Phys. Lett. 100 (20) (2012) 203120, https://doi.org/10.1063/1.4720074.

[50] J. Ma, M. Zhang, L. Dong, Y. Sun, Y. Su, Z. Xue, Z. Di, Gas sensor based on defective graphene/pristine graphene hybrid towards high sensitivity detection of NO2, AIP Adv. 9 (7) (2019) 075207, https://doi.org/10.1063/1.5099511.

[51] G. Lee, G. Yang, A. Cho, J.W. Han, J. Kim, Defect-engineered graphene chemical sensors with ultrahigh sensitivity, PCCP 18 (2016) 14198–14204, https://doi.org/10.1039/c5cp04422g.

[52] M.G. Chung, D.H. Kim, H.M. Lee, T. Kim, J.H. Choi, D.K. Seo, J.B. Yoo, S.H. Hong, T.J. Kang, Y.H. Kim, Highly sensitive NO_2 gas sensor based on ozone treated graphene, Sens Actuators B Chem. 166–167 (2012) 172–176, https://doi.org/10.1016/j.snb.2012.02.036.

[53] Y. You, J. Deng, X. Tan, N. Gorjizadeh, M. Yoshimura, S.C. Smith, V. Sahajwalla, R. K. Joshi, On the mechanism of gas adsorption for pristine, defective and functionalized graphene, PCCP 19 (2017) 6051–6056, https://doi.org/10.1039/c6cp07654h.

[54] N. Lim, H. Kim, Y. Pak, Y.T. Byun, Enhanced NO_2 sensing performance of graphene with thermally induced defects, Materials 14 (9) (2021) 2347, https://doi.org/10.3390/ma14092347.

[55] Y. Hajati, T. Blom, S.H.M. Jafri, S. Haldar, S. Bhandary, M.Z. Shoushtari, O. Eriksson, B. Sanyal, K. Leifer, Improved gas sensing activity in structurally defected bilayer graphene, Nanotechnology 23 (50) (2012) 505501, https://doi.org/10.1088/0957-4484/23/50/505501.

[56] F. Ricciardella, S. Vollebregt, R. Tilmann, O. Hartwig, C. Bartlam, P.M. Sarro, H. Sachdev, G.S. Duesberg, Influence of defect density on the gas sensing properties of multi-layered graphene grown by chemical vapor deposition, Carbon Trends. 3 (2021) 24, https://doi.org/10.1016/j.cartre.2021.10.

[57] G. Lu, S. Park, K. Yu, R.S. Ruoff, L.E. Ocola, D. Rosenmann, J. Chen, Toward practical gas sensing with highly reduced graphene oxide: a new signal processing method to circumvent run-to-run and device-to-device variations, ACS Nano 5 (2011) 1154–1164, https://doi.org/10.1021/nn102803q.

[58] E. Espid, F. Taghipour, UV-LED Photo-activated Chemical Gas Sensors: A Review, Crit. Rev. Solid State Mater. Sci. 42 (2017) 416–432, https://doi.org/10.1080/10408436.2016.1226161.

[59] P. Sun, M. Zhu, K. Wang, M. Zhong, J. Wei, D. Wu, Y. Cheng, H. Zhu, Photoinduced molecular desorption from graphene films, Appl. Phys. Lett. 101 (5) (2012) 053107, https://doi.org/10.1063/1.4742147.

[60] G. Chen, T.M. Paronyan, A.R. Harutyunyan, Sub-ppt gas detection with pristine graphene, Appl. Phys. Lett. 101 (5) (2012) 053119, https://doi.org/10.1063/1.4742327.
[61] S.-W. Fan, A.K. Srivastava, V.P. Dravid, UV-activated room-temperature gas sensing mechanism of polycrystalline ZnO, Appl. Phys. Lett. 95 (14) (2009) 142106, https://doi.org/10.1063/1.3243458.
[62] X. Yan, Y. Wu, R. Li, C. Shi, R. Moro, Y. Ma, L. Ma, High-Performance UV-assisted NO_2 sensor based on chemical vapor deposition graphene at room temperature, ACS Omega 4 (2019) 14179–14187, https://doi.org/10.1021/acsomega.9b00935.
[63] Y. Zhou, C. Gao, Y. Guo, UV assisted ultrasensitive trace NO_2 gas sensing based on few-layer MoS_2 nanosheet-ZnO nanowire heterojunctions at room temperature, J. Mater. Chem. A Mater. 6 (2018) 10286–10296, https://doi.org/10.1039/c8ta02679c.
[64] Z. Luo, N.J. Pinto, Y. Davila, A.T. Charlie Johnson, Controlled doping of graphene using ultraviolet irradiation, Appl. Phys. Lett. 100 (25) (2012) 253108, https://doi.org/10.1063/1.4729828.
[65] G. Imamura, K. Saiki, Modification of graphene/SiO_2 interface by UV-irradiation: Effect on electrical characteristics, ACS Appl. Mater. Interfaces 7 (2015) 2439–2443, https://doi.org/10.1021/am5071464.
[66] D. Ma, Y. Su, T. Tian, H. Yin, C. Zou, T. Huo, N. Hu, Z. Yang, Y. Zhang, Multichannel room-temperature gas sensors based on magnetic-field-aligned 3D Fe_3O_4@SiO_2@Reduced graphene oxide spheres, ACS Appl. Mater. Interfaces 12 (2020) 37418–37426, https://doi.org/10.1021/acsami.0c05574.
[67] G. Chen, T.M. Paronyan, E.M. Pigos, A.R. Harutyunyan, Enhanced gas sensing in pristine carbon nanotubes under continuous ultraviolet light illumination, Sci. Rep. 2 (2012), https://doi.org/10.1038/srep00343.